Biomaterials 34 (2013) 1135–1145

Contents lists available at SciVerse ScienceDirect

Biomaterials

journal homepage: www.elsevier.com/locate/biomaterials

F3 peptide-functionalized PEG-PLA nanoparticles co-administrated with tLyp-1 peptide for anti-glioma drug delivery

Quanyin Hu [a], Guangzhi Gu [a], Zhongyang Liu [a], Mengyin Jiang [d], Ting Kang [a], Deyu Miao [d], Yifan Tu [a], Zhiqing Pang [a], Qingxiang Song [b], Lei Yao [b], Huimin Xia [a,c], Hongzhan Chen [b], Xinguo Jiang [a], Xiaoling Gao [b,**], Jun Chen [a,*]

[a] Key Laboratory of Smart Drug Delivery, Ministry of Education & PLA, School of Pharmacy, Fudan University, Lane 826, Zhangheng Road, Shanghai 201203, PR China
[b] Department of Pharmacology, Institute of Medical Sciences, Shanghai Jiaotong University School of Medicine, 280 South Chongqing Road, Shanghai 200025, PR China
[c] Shanghai Institute for Food and Drug Control (SIFDC), Lane 1500, Zhangheng Road, Shanghai 201203, PR China
[d] School of Pharmacy, Shandong University of Traditional Chinese Medicine, Jinan, Shandong, PR China

ARTICLE INFO

Article history:
Received 30 September 2012
Accepted 20 October 2012
Available online 10 November 2012

Keywords:
F3 peptide
tLyp-1 peptide
Co-administration
Nanoparticle
Paclitaxel
Anti-glioma

ABSTRACT

The development of a drug delivery strategy which can mediate efficient tumor targeting together with high cellular internalization and extensive vascular extravasation is essential and important for glioma treatment. To achieve this goal, F3 peptide that specifically bind to nucleolin, which is highly expressed on the surface of both glioma cells and endothelial cells of glioma angiogenic blood vessels, is utilized to decorate a nanoparticulate drug delivery system to realize glioma cell and neovasculature dual-targeting and efficient cellular internalization. Tumor homing and penetrating peptide, tLyp-1 peptide, which contains the motif of (R/K)XX(R/K) and specially binds to neuropilin is co-administrated to improve the penetration of the nanoparticles across angiogenic vasculature into glioma parenchyma. The F3 conjugation via a maleimide–thiol coupling reaction was confirmed by XPS analysis with 1.03% nitrogen detected on the surface of the functionalized nanoparticles. Enhanced cellular interaction with C6 cells, improved penetration in 3D multicell tumor spheroids, and increased cytotoxicity of the loaded paclitaxel were achieved by the F3-functionalized nanoparticles (F3-NP). Following co-administration with tLyp-1 peptide, F3-NP displayed enhanced accumulation at the tumor site and deep penetration into the glioma parenchyma and achieved the longest survival in mice bearing intracranial C6 glioma. The findings here clearly indicated that the strategy by co-administrating a tumor homing and penetrating peptide with functionalized nanoparticles dual-targeting both glioma cells and neovasculature could significantly improve the anti-glioma drug delivery, which also hold a great promise for chemotherapy of other hard-to-cure cancers.

1. Introduction

Nowadays, the treatment of glioma, one of the most malignant brain tumors, accounting for about 42% of all brain tumors [1,2], remains a big challenge due to its highly proliferative, infiltrative and invasive property [3]. Even with aggressive treatment (surgical debulking and radiation), the prognosis of patients with malignant glioma remains dismal. Chemotherapy is the most common auxiliary treatment for glioma [4,5]. However, the efficiency of drug delivery to glioma is highly limited by the non-specific, non-targeted nature of anti-tumor agents and the presence of blood–brain barrier (BBB) and blood–brain tumor barrier (BBTB) which are extremely exclusive [6,7].

Aiming at improving the efficiency of drug delivery to glioma, various drug delivery systems (DDS) have been developed, among which nanoparticulate DDS have attracted increasing interest as they can be used to improve drug delivery and efficacy by incorporating multiple functions and increasing the payload [8,9]. However, the dysfunctional tumor blood vessels, high interstitial pressure and the much smaller pore size for solute passage in glioma than that in peripheral tumors tend to prevent penetration of drugs and nanoparticles into the tumor sites, and thus limit the efficacy of the treatments [10–12]. Although active-targeting based on tumor-specific molecules such as antibodies and peptides that

* Corresponding author. Tel.: +86 21 51980066; fax: +86 (0)21 51980069.
** Corresponding author. Tel.: +86 21 63846590x778015
E-mail addresses: shellygao1@yahoo.com.cn (X. Gao), chenjun@fudan.edu.cn, chenjun_1974@yahoo.com.cn (J. Chen).

0142-9612/$ – see front matter © 2012 Elsevier Ltd. All rights reserved.
http://dx.doi.org/10.1016/j.biomaterials.2012.10.048

specifically bind to receptors expressed at high levels on glioma vasculature or glioma cells has helped in rendering targeted recognization and binding of nanoparticulate DDS at the tumors sites [13,14], the lack of effective cellular internalization and disability in penetrating through the endothelial cells of blood vessels and distributing into the glioma parenchyma remain to be the major obstacle to anti-glioma drug delivery. Development of nanoparticulate DDS with efficient tumor targeting together with high cellular internalization and extensive extravasation will significantly improve the therapeutic efficacy of anti-cancer agents against glioma.

Nucleolin, a shuttle protein that traffics between cell membrane and nucleus, is overexpressed on the surface of both glioma cells and endothelial cells of angiogenic blood vessels, but only exist in the nucleus among normal cells [15], offering an attractive target for mediating specific and efficient angiogenic blood vessels and glioma cells dual-targeting together with high cellular internalization. F3 peptide, discovered by using phage-displayed cDNA libraries [16], can specifically bind to cell surface nucleolin and undergo an effective cell surface to nucleus transport. Here we speculated that F3 peptide can be utilized as an effective ligand to mediate the site-specific accumulation and internalization of PEG-PLA nanoparticles at the location of glioma.

Efficacy of active-targeting nanoparticulate DDS in glioma therapy is also limited by its low extravasation from the blood vessels and penetration into the glioma parenchyma [17,18] due to the small pore size for penetration in glioma. Dortor Ruoslahti's group has recently reported a technique that can overcome this problem, in which C-end Rule (CendR) peptides that containing the motif of (R/K)XX(R/K) (X represents any amino acid) can induce extravasation and tissue penetration via a mechanism that involves cell internalization [19]. The receptor for the CendR motif is neuropilin-1 (NRP1) which is a transmembrane protein overexpressed on the surface of endothelial cells of tumor blood vessels [20]. tLyp-1, a tumor homing peptide, also contains a CendR motif and has been reported to be able to mediate tissue penetration through the neuropilin-1-dependent internalization pathway [21]. As co-administration with tumor-penetrating peptide will bypass the modification of peptide on the surface of nanoparticulate DDS, will not influence the activity of peptide, and will not be limited by the finite number of target receptors, and is expected to result in triggering a bulk transfer of the bystander DDS into the tumor parenchyma, here we proposed that co-administration tLyp-1 peptide with the F3-functionalized nanoparticles might provide an effective strategy to mediate specific tumor targeting, high cellular internalization and extensive extravasation for anti-glioma drug delivery.

In order to justify this hypothesis, PEG-PLA nanoparticles were prepared with an emulsion/evaporation method, loaded with paclitaxel (PTX) as the model drug, surface functionalized with F3 peptide and co-administered with tLyP-1 with both *in vitro* and *in vivo* tumor targeting, cellular uptake, glioma vascular extravasation, and anti-glioma efficacy evaluated.

2. Materials and methods

2.1. Materials

Methoxy-poly(ethylene glycol) $_{3000}$-poly(lactic acid) $_{34000}$ (MePEG-PLA) and maleimide-poly(ethylene glycol) $_{3400}$-poly(lactic acid) $_{34000}$ (Male-PEG-PLA) were kindly provided by East China University of Science and Technology. PTX were purchased from Xi'an Sanjiang Biological Engineering Co. Ltd (Xi'an, China), and Taxol® from Bristol-Myers Squibb Company. Coumarin-6 and DiR (1, 1′-dioctadecyl -3, 3, 3′, 3′-tetramethyl indotricarbocyanine Iodide) were purchased from Sigma–Aldrich (St. Louis, MO, USA). DAPI (4, 6-diamidino-2-phenylindole) was obtained from Molecular Probes (Eugene, OR, USA), cell counting kit-8 (CCK-8) was provided by Dojindo Laboratories (Kumamoto, Japan) and BCA protein assay kit by Pierce (Rockford, IL, USA). All other reagents were of analytical or chromatographic pure grade and purchased from Sinopharm Chemical Reagent Co., Ltd (Shanghai, China).

F3 peptide (CKDEPQRRSARLSAKPAPPKPEPKPKKAPAKK) was synthesized by Shanghai Mocell Biotech Co., Ltd (China), and tLyp-1 peptide (CGNKRTR) obtained from ChinaPeptides Co., Ltd (Shanghai, China).

Dulbecco's Modified Eagle's Medium (DMEM), fetal bovine serum (FBS), 0.25% trypsin-EDTA, penicillin–streptomycin and non-essential amino acid were purchased from Gibco BRL (Carlsbad, CA, USA).

Rat C6 glioma cell lines were provided by Cell Institute of Chinese Academy of Sciences (Shanghai, China).

Male Sprague-Dawley rats (200 ± 20 g), Balb/c nude mice (male, 4–5 weeks, 20 ± 2 g) were obtained from BK Lab Anima Ltd. (Shanghai, China) and housed at 25 ± 1 °C with free access to food and water. The protocol of animal experiments was approved by the Animal Experimentation Ethics Committee of Fudan University.

2.2. Preparation of F3-functionalized nanoparticles

The nanoparticles (NP) loaded with PTX was prepared through the emulsion/solvent evaporation technique according to the procedure described previously [22]. Firstly, 22.5 mg MePEG-PLA, 2.5 mg Male-PEG-PLA and 1% of PTX (g/g) were dissolved in 1 ml dichloromethane, followed by the addition of 2 ml of 1% sodium cholate aqueous solution, emulsified by sonication (280 w, 30 s) with probe sonicator (Ningbo Scientz Biotechnology Co. Ltd., China) in ice water bath. Then the emulsion was added into 8 ml of 0.5% sodium cholate aqueous solution under rapid magnetic stirring for 5 min. The emulsion was subsequently applied to a rotary evaporator (Shanghai Institute of Organic Chemistry, China) to remove the dichloromethane and concentrated by centrifugation at 21,000 g for 45 min using TJ-25 centrifuge (Beckman Counter, USA). After discarding the supernatant, the nanoparticles were resuspended in distilled water and then subjected into a 1.5 × 20 cm sepharose CL-4B column (Pharmacia Biotech, Inc., Sweden) and eluted with 0.01 M HEPES buffer (pH 7.0) to remove the unencapsulated PTX. F3-functionalized nanoparticles (F3-NP) was prepared via a maleimide–thiol coupling reaction at room temperature for 6 h. The products were then eluted with distilled water through the 1.5 × 20 cm sepharose CL-4B column to remove the unconjugated peptides. Blank nanoparticles were prepared as described above without adding PTX. Coumarin-6-labeled and DiR-labeled nanoparticles were prepared with the same procedure except for containing coumarin-6 and DiR.

2.3. Characterization of the nanoparticles

2.3.1. Particle size and zeta potential

Particle size and zeta potential of PTX-labeled NP (NP-PTX) and PTX-labeled F3-NP (F3-NP-PTX) were determined by dynamic light scattering (DLS) analysis using Zeta Potential/Particle Sizer NICOMP380 ZLS (Santa Barbara, California, USA.) with He–Ne lamp at 632.8 nm.

2.3.2. Transmission electron microscopy

The morphological examination of nanoparticles was performed under a transmission electron microscope (TEM) (H-600, Hitachi, Japan) following negative staining with sodium phosphotungstate solution.

2.3.3. Encapsulation efficiency and drug loading capacity

The encapsulation efficiency (EE) and loading capacity (LC) of PTX in NP-PTX and F3-NP-PTX was determined by high performance liquid chromatography (HPLC). The EE% and LC% were calculated as indicated below ($n = 3$).

$$\text{EE}\ (\%) = \frac{\text{PTX in the nanoparticles}}{\text{Total amount of PTX in dispersion}} \times 100\%$$

$$\text{LC}\ (\%) = \frac{\text{Amount of PTX in nanoparticles}}{\text{nanoparticles weight}} \times 100\%$$

2.3.4. F3 conjugation efficiency and F3 density on nanoparticle surface

To determine the F3 conjugation efficiency, 20 μl aliquots of F3-NP and NP (dissolved in PBS pH 7.4) were added in triplicate wells (96-well plate), followed by the addition of 160 μl BCA Protein Assay Reagent, respectively. After 1 h incubation at 37 °C, the absorption was measured via a microplate reader (Thermo Multiskan MK3, USA) at 562 nm.

F3 conjugation efficiency (CE%) was calculated to determine the percentage of F3 peptide conjugated to the nanoparticles surface. The calculation formula was as follows:

$$\text{CE}\ (\%) = \frac{\text{Amount of F3 conjugated on the surface of nanoparticle}}{\text{Total amount of F3 added}} \times 100\%$$

F3 peptide surface density (S) was calculated by dividing the number of F3 molecules by the calculated average number (n) of nanoparticles which was determined by the methods described by Olivier et al. [23] $n = 6 * m/(\pi * D^3 * \rho)$, in

which m is the nanoparticle weight, D is the number-based mean nanoparticle diameter, and ρ is the nanoparticle weight per volume unit (density), estimated to be 1.1 g/cm^3 [24].

2.3.5. X-ray photo electron spectroscopy (XPS)

To determine the surface composition of NP and F3-NP, the samples were lyophilized by using an ALPHA 2-4 Freeze Dryer (0.070 Mbar Vakuum, −80 °C, Martin Christ, Germany) and then subjected to XPS analysis. The determination was performed on a RBD upgraded PHI-5000C ESCA system (Perkin Elmer).

2.4. In vitro PTX release

In vitro PTX release from NP, F3-NP and Taxol® was evaluated with an equilibrium dialysis method [25] using phosphate buffer solution (PBS, pH 7.4) containing 0.1% (v/v) Tween-80 as the release media. For the experiment, 1 ml of the freshly prepared NPs loaded with PTX (0.1 mg) and commensurate Taxol® were added into a dialysis bag (MWCO = 8000 Da, Greenbird Inc., Shanghai, China), which was then immersed in 30 ml release medium and incubated at 37 °C at the shaking speed of 100 rpm. At pre-decided time points (1, 2, 3, 4, 6, 8, 12, 24, 48, 72, 96 h), 0.2 ml aliquots were withdrawn and replaced with an equal volume of fresh medium. The aliquots then subjected to HPLC analysis as described previously [26].

2.5. Cell experiments

2.5.1. Cell culture

C6 glioma cells were cultured in DMEM containing 10% fetal bovine serum, 100 U/ml penicillin and 100 μg/ml streptomycin at 37 °C in a 5% CO_2/95% air humidified environment incubator (Thermo HERAcell®, USA).

2.5.2. Cellular association of coumarin-6-labeled NPs

C6 cells were seeded into a 96-well plate at the density of 5000 cells per well. For qualitative experiment, after 24 h incubation, the medium was replaced with different concentrations of coumarin-6-labeled nanoparticles (25–200 μg/ml). After a 2-h incubation, the cells were washed twice with cold PBS buffer, fixed with 4% formaldehyde for 15 min, and then subjected to fluorescent microscopy analysis (Leica DMI4000 B, Germany). For quantitative experiment, the cells were incubated with 200 μg/ml nanoparticles for a period of time (from 0.5 to 8 h). After fixation, the cells were stained with 2 μg/ml Hochest 33258 at room temperature for 20 min away from light, washed twice with cold PBS and then subjected to quantitative analysis via a KineticScan HCS Reader (version 3.1, Cellomics Inc., Pittsburgh, PA, USA) as described previously [27]. In order to clarify whether the uptake process was energy relevant, the cellular association experiments were performed at 37 °C, and 4 °C, respectively, at the nanoparticle concentration from 25 to 600 μg/ml.

In the inhibition experiment, the cells were seeded in a 96-well plate (5000 cells per well). Twenty-four hours later, the medium was changed to 100 μl different inhibitors (10 μg/ml chlorpromazine, 4 μg/ml colchicines, 10 μg/ml cyto-D, 5 μg/ml BFA, 5 μg/ml filipin, 10 mM NaN_3, 50 mM deoxyglucose, 2.5 mM methyl-β-cyclodextrin (M-β-CD), 200 nM monensin, 20 μM nocodazole or 100 μg F3 peptide). After that, the cells were incubated with 200 μg/ml nanoparticles for 2 h at 37 °C, and the cells were treated as described above for quantitative analysis.

2.5.3. In vitro anti-proliferation efficiency

In order to evaluate the cytotoxicity of the F3-NP on C6 cells, the cells were seeded in a 96-well plate at a density of 5000 cells per well. Twenty-four hours later, the medium was substituted with different concentration of nanoparticles (0.001, 0.01, 0.05, 0.1, 0.8, 1 and 10 μg/ml) for 72 h. To determine the anti-proliferation effect of the nanoparticles in the presence of tLyp-1, 100 μg tLyp-1 peptide was added into

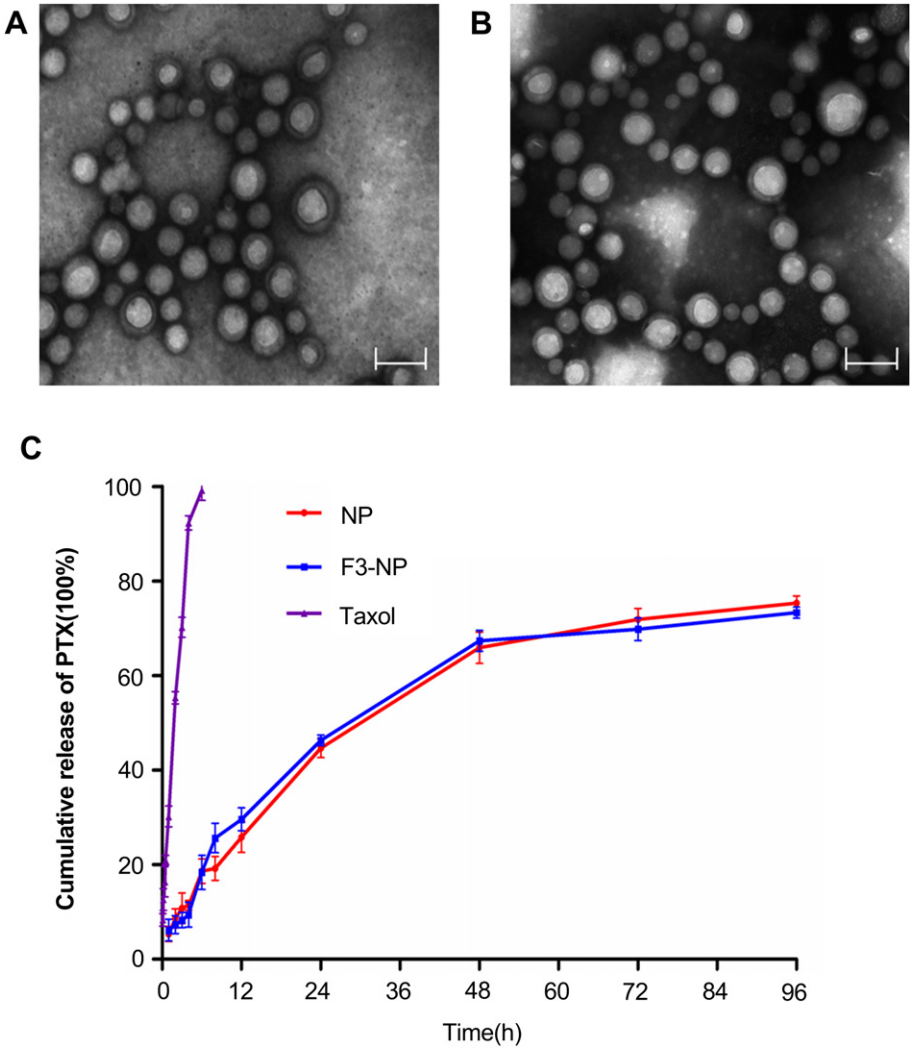

Fig. 1. TEM images of (A) unmodified NP and (B) F3-NP. Bar: 200 nm. (C) *In vitro* cumulative release of PTX from Taxol®, NP-PTX and F3-NP-PTX in PBS (pH 7.4) with 0.1% Tween-80 at 37 °C.

Table 1
Characterization of NP and F3-NP. Data represented mean ± SD ($n = 3$).

Nanoparticles	Particle size (nm)	Polydispersityindex (PI)	Zeta potential (mV)
NP	100 ± 12.35	0.11 ± 0.05	−32.5 ± 3.56
F3-NP	125 ± 11.12	0.26 ± 0.13	−13.3 ± 1.32

the wells and incubated with the cells together with F3-NP at 37 °C. For cell viability analysis, 100 μl fresh medium was added into wells, followed by the addition of 10 μl CCK-8. After 1 h incubation, the absorption which represented cell viability was measured via a microplate reader (Thermo Multiskan MK3, USA) at the wavelength of 450 nm.

2.5.4. Penetration in tumor spheroids

In order to evaluate the tumor-penetrating ability of F3-NP, C6 cells were seeded in a 48-well plate pre-coated with 150 μl of 2% agarose (low melting point) at a density of 2000 cells/well to prepare the 3D tumor spheroids [28]. After cultured for 7 days, 400 μg/ml NP and F3-NP loaded with coumarin-6 were incubated with the tumor spheroids in the absence/presence of 200 μg tLyp-1 peptide at 37 °C for 4 h. After that, the tumor spheroids were rinsed with cold PBS and fixed with 4% formaldehyde and then subjected to laser scanning confocal microscopy analysis (LSM510, Leica, Germany).

2.6. In vivo experiments

2.6.1. In vivo real-time imaging

To track the *in vivo* real-time distribution of the nanoparticles, DiR was used as the fluorescent probe as described previously [29]. The mice bearing intracranial C6 glioma, prepared by intracranially injected C6 cells (5×10^5 cells/5 μl in pH 7.4 PBS) into the right brain of each nude mouse and cultured for fourteen days, were divided into four groups. NP, F3-NP were injected into mice at the dose of PTX 5 mg/kg, and the co-adminstration peptide tLyp-1 were given at the dose of 4 μM/kg 5 min after the NPs injection. After the treatment, the animals were subjected to a MAESTRO small live animal imaging system (CRi, MA, USA) and imaged at predetermined time points. Twenty-four hours after injection, the mice were sacrificed with the brains and other organs collected and imaged.

2.6.2. In vivo glioma distribution

The mice model bearing intracranial C6 glioma were obtained as described above, and housed at standard condition for 2 weeks. Coumarin-6-labeled NP, F3-NP and NP and F3-NP co-administrated with peptide tLyP-1 were given to the animals intravenously. Three hours later, the mice were anesthetized and heart perfused with saline and 4% paraformaldehyde with the brains obtained. Afterwards, the brains were further fixed in 4% paraformaldehyde, dehydrated with 10%, 30% sucrose solution, embedded in OCT (Sakura, Torrance, CA, USA) and frozen sectioned. Finally, the slides were stained with DAPI and subjected to confocal microscopy analysis (LSM710, Leica, Germany).

2.6.3. Pharmacokinetic studies

Twelve SD rats (200 ± 20 g) were used for pharmacokinetic studies, randomly divided into four groups ($n = 3$) and given Taxol®, NP-PTX, F3-NP-PTX, and F3-NP-PTX with co-administration of tLyp-1, respectively, at the PTX dose 5 mg/kg and tLyp-1 dose 4 μM/kg. At the predetermined time points (0.083, 0.25, 0.5, 1, 2, 4, 6, 8, 12, 24 h), blood samples were collected from the carotid vein and centrifugated at 3000 rpm for 10 min with the supernatant stored at −20 °C until assay.

To prepare samples for analysis, 200 μl methanol containing 60 ng/ml docetaxel (internal standard) was added into 50 μl plasma to precipitate the proteins. The mixture was vortexed and subsequently centrifuged at 12,000 rpm for 10 min with the supernatant mixed with an equal volume of deionized water and subjected to liquid chromatography–tandem mass spectrometry (LC–MS/MS) analysis as described previously [30]. Detection of the ions was conducted in the multiple reaction monitoring (MRM) mode, monitoring the transition of the m/z 876.6 → 308.0 for paclitaxel $(M + Na)^+$ and 830.3 → 549.1 for docetaxel $(M + Na)^+$, respectively. All the concentration data were dose-normalized and plotted as plasma drug concentration–time curves. The pharmacokinetic data analysis was performed by means of a model independent method [31].

2.6.4. Anti-glioma efficacy

The mice model bearing intracranial C6 glioma were established as described above, randomly divided into six groups ($n = 6$) and intravenously given Taxol®, NP-PTX, NP-PTX with co-administration of tLyp-1 peptide, F3-NP-PTX,

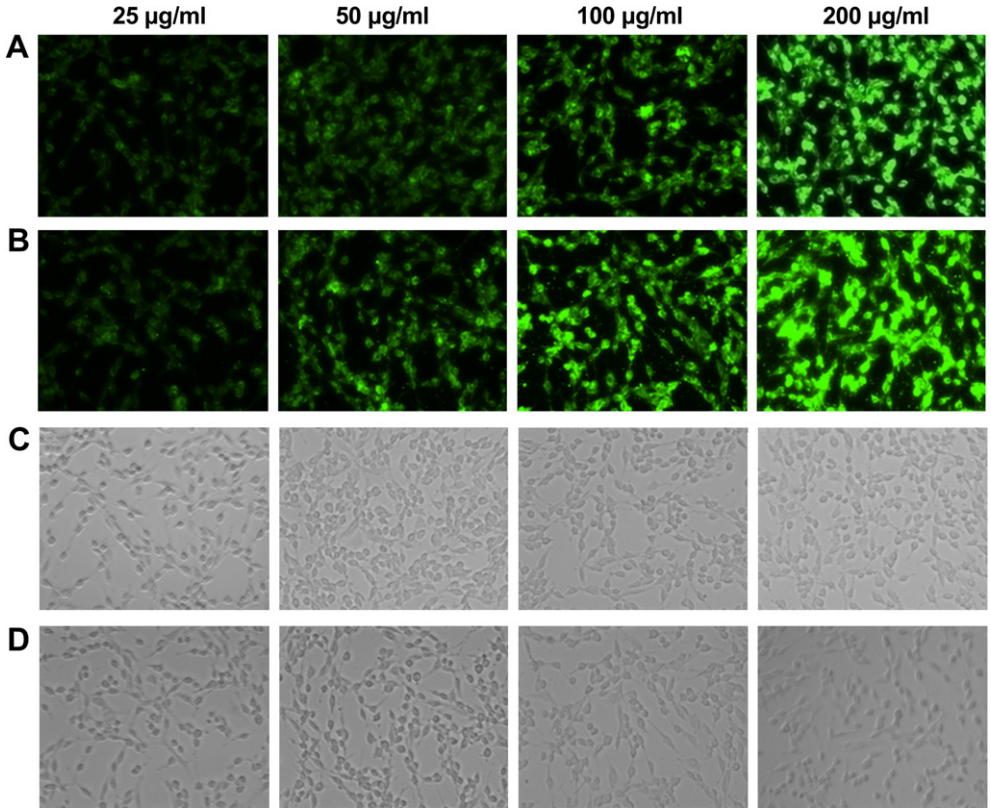

Fig. 2. Cellular uptake of coumarin-6-labeled (A) unmodified NP and (B) F3-NP (green) in C6 cells after incubation for 2 h at the concentration ranged from 25 to 200 μg/ml. (C) Bright field image of C6 cells treated with NP, and (D) Bright field image of C6 cells treated with F3-NP. Original magnification: 20×. (For interpretation of the references to color in this figure legend, the reader is referred to the web version of this article.)

F3-NP-PTX with co-administration of tLyP-1 peptide (PTX dose 5 mg/kg, tLyp-1 dose 4 μM/kg) and saline, respectively, every three days for two weeks. The anti-glioma efficacy of the formulations was evaluated by measuring the survival of the animals after the treatments.

2.7. Statistical analysis

All the data were presented as mean ± SD unless otherwise indicated. Unpaired student's *t* test was used for between two-group comparison and one-way ANOVA with Bonferroni tests for multiple-group analysis. Statistical significance was defined as $p < 0.05$.

3. Results

3.1. Characterization of NP and F3-NP

The nanoparticles were prepared via emulsion/solvent evaporation, and F3-NP was obtained via a maleimide–thiol coupling reaction. The F3 conjugation slightly increased the particle size (125 ± 11.12 nm). Transmission electron micrographs showed the same spherical shape of NP and F3-NP (Fig. 1A, B) (Table 1). Encapsulation of PTX, coumarin-6 and DiR did not change the particle size. After modification, zeta potential of F3-NP was significantly increased as F3 peptide contained several positive charge amino acids. Also the existence of F3 peptide on the surface of F3-NP was confirmed by XPS analysis which showed 1.03% nitrogen on the surface of F3-NP while that on the unmodified NP was under the limit of detection.

The LC of NP and F3-NP was 1.53 ± 0.03% and 1.37 ± 0.06%, respectively, with the EE 48.3 ± 2.3% and 47.6 ± 1.6%, respectively.

Under the our experimental conditions (weight ratio of Male-PEG-PLA to MPEG-PLA 1: 9, molar ratio of mal-PEG-PLA to F3 1: 1, incubation time for conjugation reaction 6 h), the F3 peptide-conjugation efficiency was 48.5 ± 2.3%, and the F3 peptide density on the nanoparticle surface was 526 ± 52.

3.2. In vitro PTX release

In vitro release experiment showed that the NP formulations (NP-PTX and F3-NP-PTX) present almost the same release behavior (Fig. 1C). In the first 6 h, a burst release was achieved for both of the formulations. Twenty-four hours later, the release rate slowed down. At the end of 96 h, the cumulative release of PTX from NP was 74.83 ± 2.68%, and that from F3-NP-PTX was 73.59 ± 1.73%. In contrast, more than 96% PTX released from Taxol® within 4 h.

3.3. Cell experiments

3.3.1. Cell association of nanoparticles

Cellular uptake experiments were performed qualitatively via fluorescent microscopy analysis using coumarin-6 as the fluorescent probe. As shown in Fig. 2, the cellular associated fluorescence intensity of F3-NP was significantly higher than that of NP.

Quantitative analysis showed that C6 cells uptake was concentration and temperature-dependent, and the C6 cell uptake of F3-NP were 2.0, 2.3, 2.7, 4.9, 5.35 6.23 folds when compared with that of the unmodified NP at 37 °C at the nanoparticle concentration of 100, 150, 200, 300, 400, 500 and 600 μg/ml, respectively (Fig. 3).

Inhibition experiment showed that the cellular uptake of NP was inhibited by M-β-CD, while that of F3-NP was restricted by M-β-CD, nocodazole and BFA. In addition, pre-added F3 peptide also competitively and significantly inhibited the cellular uptake of F3-NP but not the unmodified NP (Fig. 4).

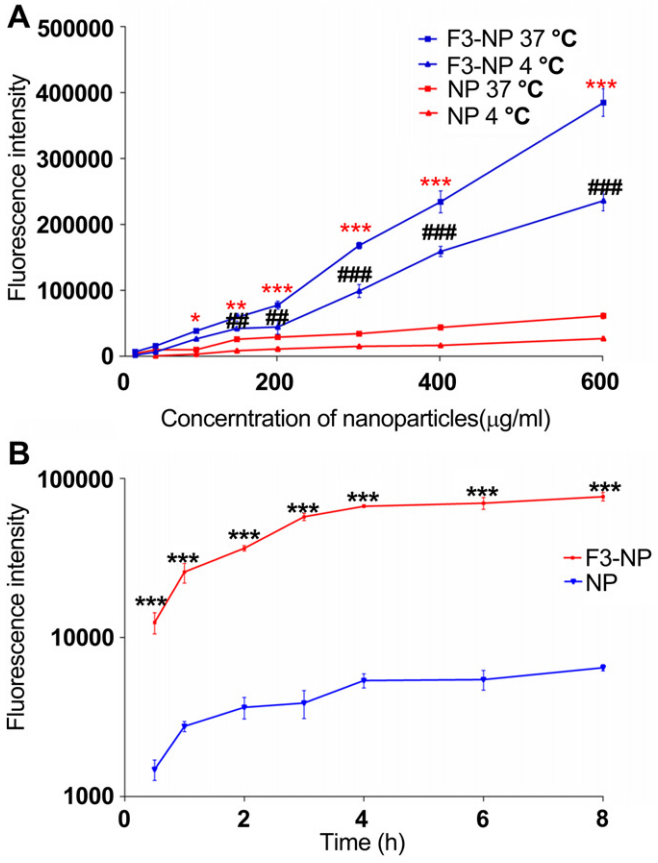

Fig. 3. (A) Cellular uptake of coumarin-6-labeled unmodified NP and F3-NP in C6 cells at different temperature (4 °C and 37 °C) after incubation for 2 h at the nanoparticle concentrations from 25 μg/ml to 600 μg/ml. (B) Cellular uptake of coumarin-6-labeled NP and F3-NP in C6 cells after incubation for 0.5 h–8 h at the NPs concentration of 200 μg/ml. Data represented mean ± SD ($n = 3$). $^{*}p < 0.05$, $^{**}p < 0.01$, $^{***}p < 0.001$ significantly higher than the cellular uptake of unmodified NP at 37 °C, and $\#p < 0.05$, $\#\#p < 0.01$, $\#\#\#p < 0.001$ significantly higher than the cellular uptake of unmodified NP at 4 °C.

3.3.2. In vitro anti-proliferation effect

To evaluate the anti-proliferation effect of the PTX formulations on malignant glioma C6 cells, Taxol®, NP-PTX, F3-NP-PTX and F3-NP-PTX with tLyp-1 were incubated with C6 cells, respectively, for 72 h with the cell viability detected by a CCK-8 analysis. The IC_{50} were 0.403 μg/ml for Taxol®, 0.207 μg/ml for NP-PTX, 0.075 μg/ml for F3-NP-PTX and 0.070 μg/ml for F3-NP-PTX in the presence of tLyp-1.

3.3.3. Penetration in tumor spheroids

The penetrating ability of F3-NP was evaluated *in vitro* in 3D tumor spheroids. As showed by confocal microscopy analysis, F3-NP distributed more extensive than NP in the 3D tumor spheroids (Fig. 5A, C). Quantitative analysis showed that the penetration depth of F3-NP was 139.26 μm while that of NP was only 81.02 μm (Fig. 5B, D). On the other hand, the addition of tLyp-1 peptide did not enhance the penetrating ability of F3-NP (133.89 μm in depth) in the avascular tumor spheroids (Fig. 5).

3.4. In vivo experiments

3.4.1. In vivo real-time imaging

Intravital near-infrared (NIR) imaging experiment was performed to evaluate the targeting ability of F3 peptide and the effect of co-administration with tLyp-1 peptide. It was showed that at the

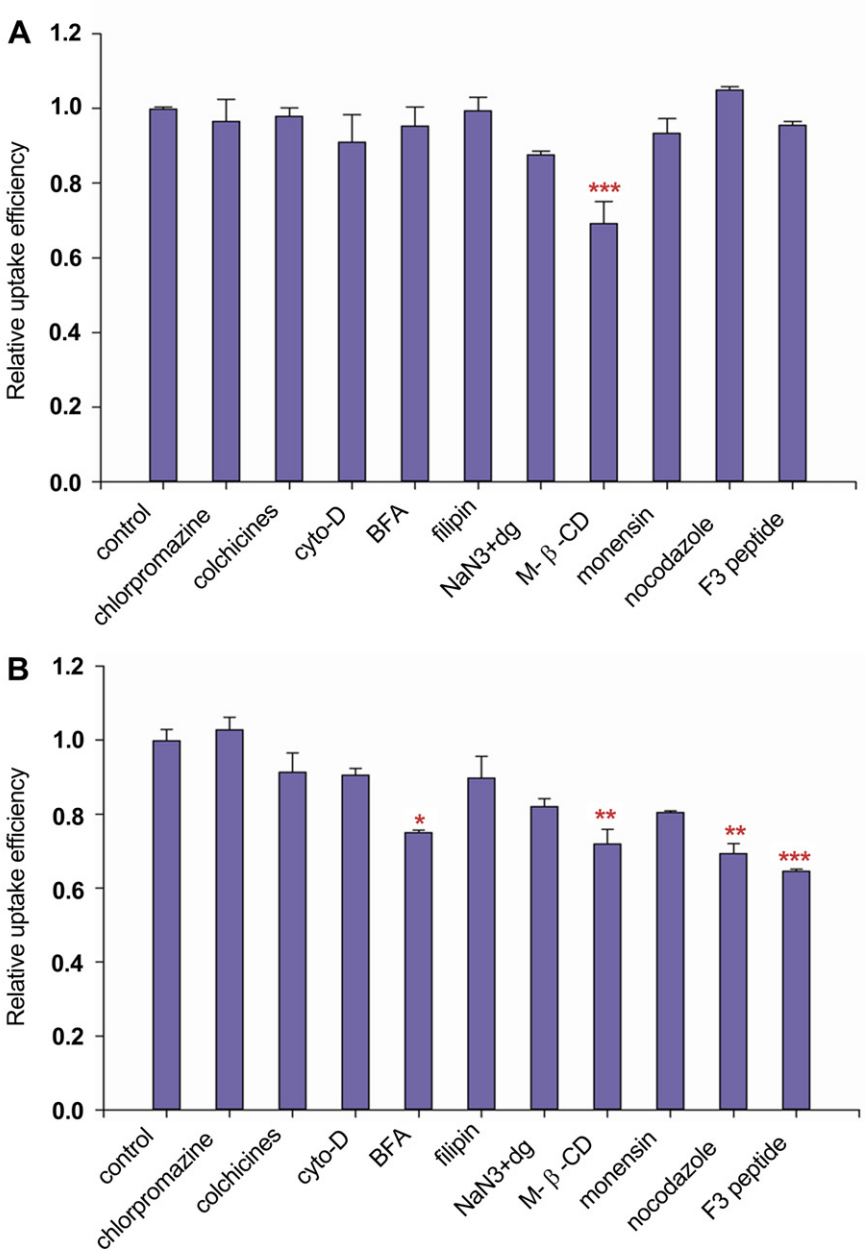

Fig. 4. Cellular association of coumarin-6-labeled (A) NP and (B) F3-NP in the presence of different endocytosis inhibitors. Data represented mean ± SD ($n = 3$). $^{*}p < 0.05$, $^{**}p < 0.01$, $^{***}p < 0.001$ significantly different with that of the non-inhibited control.

tumor locations, F3-NP with co-administration of tLyp-1 showed much higher fluorescent intensity than the other three formulations at all the time points post-injection, and the glioma-targeting efficiency followed the order: F3-NP with tLyp-1 > F3-NP > NP with tLyp-1 > NP. This result was confirmed by imaging those brains taken out from mice bearing intracranial glioma 24 h post-injection (Fig. 6).

3.4.2. *In vivo glioma distribution*

After implanting C6 glioma cells into the right striatum of nude mice, the infiltrative growth of C6 cells brought out a vivid boundary between normal brain tissue and glioma (tumor cell nucleuses were pyknotic, while that of normal brain tissue were sparse) (Fig. 7). A low NP distribution was observed at the site of glioma and mostly located at the edge of the tumor (Fig. 7A). In contrast, a significant higher distribution and deeper penetration was achieved by F3-NP (Fig. 7C). For NP co-administrated with tLyP-1 peptide, a deeper distribution into the glioma was observed when compared with both NP and F3-NP, although the whole fluorescent intensity was still slightly weaker than that of F3-NP (Fig. 7B). In contrast, F3-NP co-administrated with tLyp-1 presented the highest accumulation and deepest penetration at the location of glioma (Fig. 7D).

3.4.3. *Pharmacokinetic studies*

Plasma concentration–time curves of different PTX formulations after intravenous administration at the PTX dose 5 mg/kg and tLyp-1 dose 4 μM/kg were shown in Fig. 8. As expected, Taxol® displayed the rapidest clearance *in vivo*. At 12 h post-injection, the concentration of PTX of the Taxol® group was already under the limit of detection. In contrast, the NPs-based formulations showed much higher concentration at all time points. Significantly

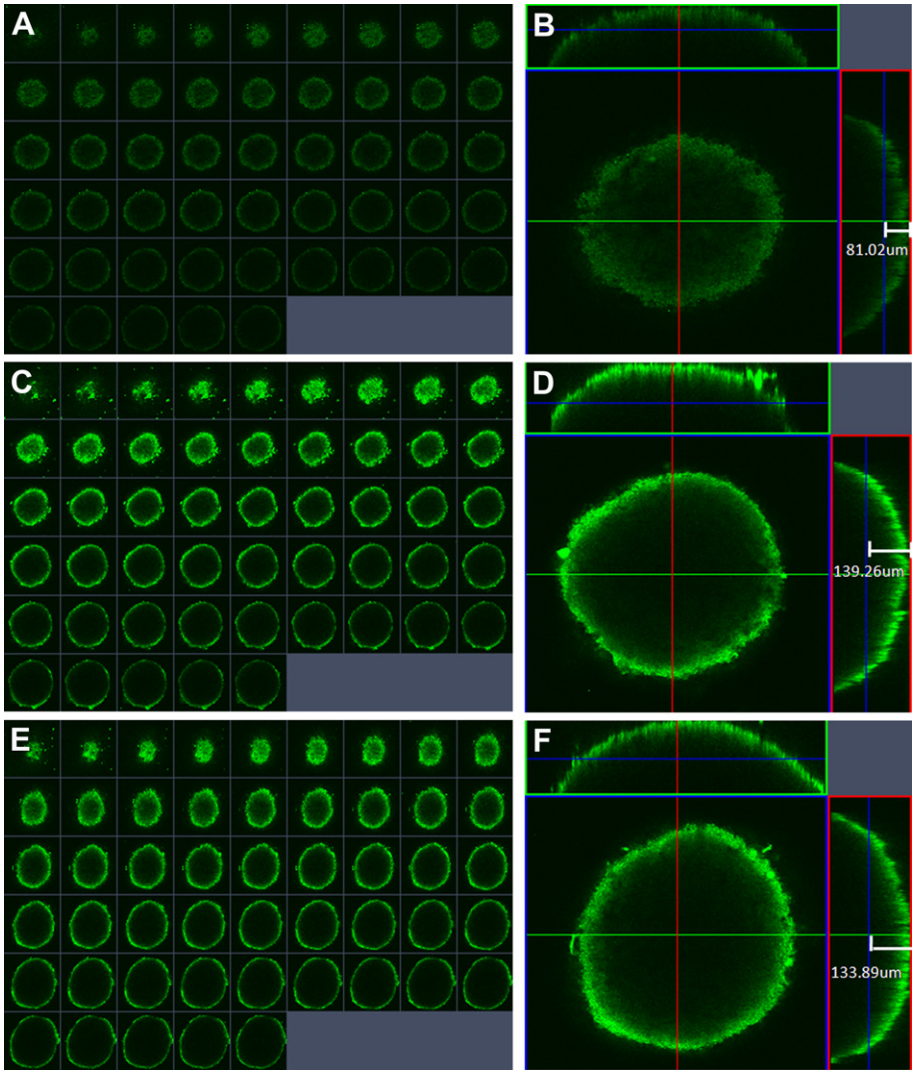

Fig. 5. Confocal microscopy analysis of the nanoparticle penetration in 3D tumor spheroids. A, C, E, multi-level scan of the penetration of NP, F3-NP, and F3-NP with tLyp-1, respectively, the interval between the consecutive slides was 5 μm. B, D, F, quantitative measurement of the penetration depth of NP, F3-NP, and F3-NP with tLyp-1, respectively.

prolonged elimination half-life ($t_{1/2}$), decreased clearance rate (CL) and enlarged $AUC_{0-24\ h}$ were achieved for all the NPs formulations (Table 2). No significant differences were found between NP-PTX and F3-NP-PTX. Co-administration with tLyp-1 peptide did not change the circulation behavior of F3-NP-PTX.

3.4.4. Anti-glioma efficacy

Anti-glioma efficacy was evaluated by survival experiment performed on mice bearing intracranial C6 glioma. The medium survival was 19 days for those animals treated with saline, 24 days with Taxol®, 27 days with NP, 32 days with F3-NP, 31 days with NP and tLyp-1, and 42 days with F3-NP and tLyp-1 (Fig. 9). Additionally, log-rank analysis showed that F3-NP with co-administration of tLyp-1 significantly prolonged the survival of mice bearing glioma when compared with F3-NP ($p < 0.05$), NP and tLyp-1 ($p < 0.01$), NP ($p < 0.001$), Taxol® ($p < 0.001$), and saline ($p < 0.001$) (Table 3).

4. Discussion

Despite advances in surgical and medical therapy, glioma remains a most fatal disease and its treatment outcomes are mostly unsatisfactory. Neurosurgery could not remove all cancerous cells due to the aggressive and infiltrative growth of glioma and its histological similarities to glial cells, including astrocytes and oligodendrocytes [32]. The currently available anti-glioma therapeutics is less than optimal for glioma treatment, mainly owing to the delivery problems. Nanoparticles show many advantages when used for delivering anti-cancer agents owing to their ability to cross multiple biological barriers, protect the drug from degradation, release a therapeutic payload in the optimal dosage range and enable the delivery of the therapeutic agent to a preferential site, realizing a targeted delivery [33], especially for glioma treatment. However, glioma presents distinguished specificity in contrast to the other types of tumors, BBB and BBTB doubly hamper the therapeutic efficacy of anti-tumor drugs and/or drug delivery systems.

Many strategies toward the treatment of glioma have been developed over the past few years, including overcoming blood–brain barrier [34,35], blood–brain tumor barrier [36] or/and targeting glioma cells [14,37–39], among which that overcoming BBTB provides the greatest advantages as BBTB becomes the main obstacle to anti-glioma DDS with the development of brain tumors and the gradual impairment of BBB. As angiogenesis, a pathological hallmark of BBTB formation, is a critical step during tumorigenesis, evasion

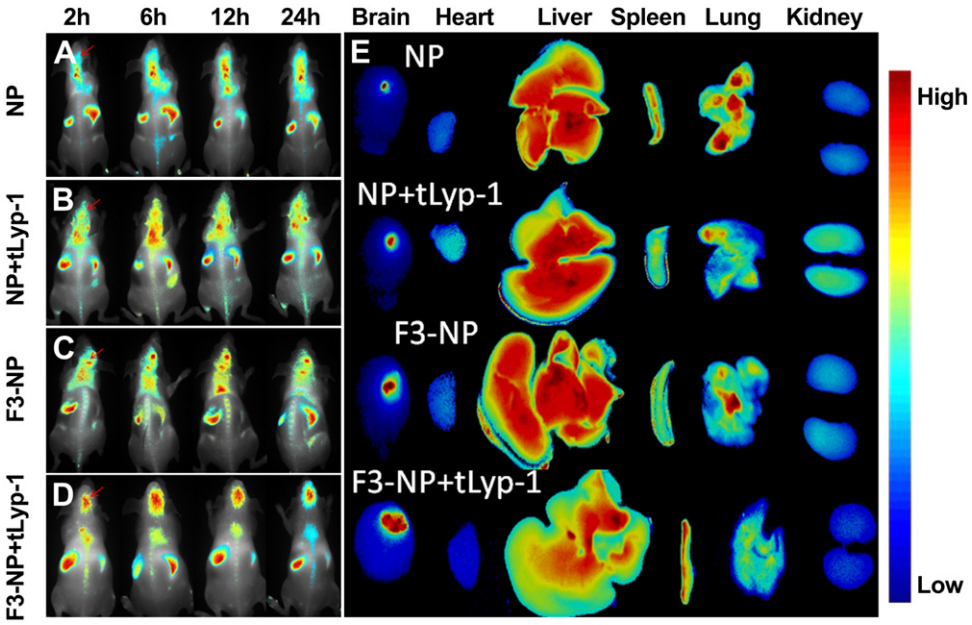

Fig. 6. *In vivo* real-time NIR fluorescent imaging of mice bearing intracranial C6 glioma which were intravenously injected with (A) NP, (B) NP with tLyp-1, (C) F3-NP, and (D) F3-NP with tLyp-1 at predetermined time points. (E) Distribution of the fluorescent signals from the NPs in various organs 24 h post-injection. All the NP formulations were loaded with DiR as fluorescent probe and the red arrows represented the site of glioma. (For interpretation of the references to color in this figure legend, the reader is referred to the web version of this article.)

and metastasis [40], it was speculated that angiogenesis vascular and glioma cells dual-targeting strategy offers the possibility to achieve more specific and effective anti-glioma drug delivery. In this contribution, the targeting receptor of F3 peptide – nucleolin was overexpressed on the surface of both endothelial cells of angiogenic blood vessels and glioma cells, but only existed in the nucleus among normal cells. Therefore, F3-functionalized DDS would achieve excellent dual-targeting efficiency and high internalization by glioma cells together with reduced side effect on normal cells. Furthermore, a key supplementary by co-administrating F3-NP with tLyp-1 peptide was made to increase extravasation of the DDS from the angiogenic blood vessels and penetrated into the tumor parenchyma. This strategy was expected to provide a safe and efficient platform for the anti-glioma drug delivery.

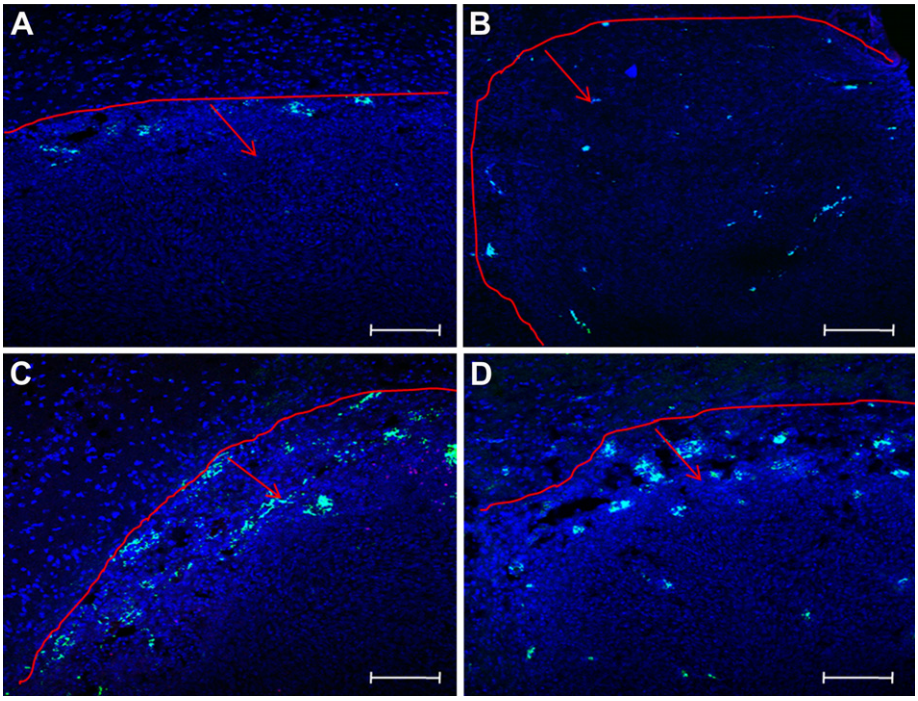

Fig. 7. *In vivo* glioma distribution of (A) NP, (B) NP with tLyp-1, (C) F3-NP and (D) F3-NP with tLyp-1 3 h after tail vein injection. Red lines showed the boundary between glioma and normal brain tissue. Arrows indicated the glioma zones. Bar: 100 μm. (For interpretation of the references to color in this figure legend, the reader is referred to the web version of this article.)

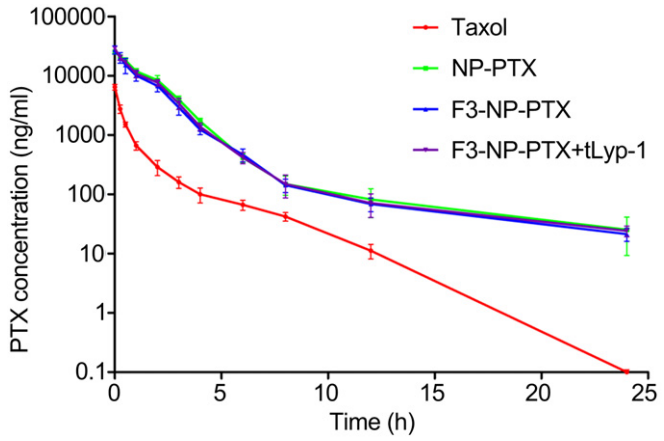

Fig. 8. Plasma PTX concentration–time curves after i.v. administration of Taxol®, NP-PTX, F3-NP-PTX and F3-NP-PTX with co-administration of tLyp-1 peptide to SD rats at 5 mg/kg PTX dose and 4 μM/kg tLyp-1 dose, respectively. Data represented mean ± SD ($n = 3$).

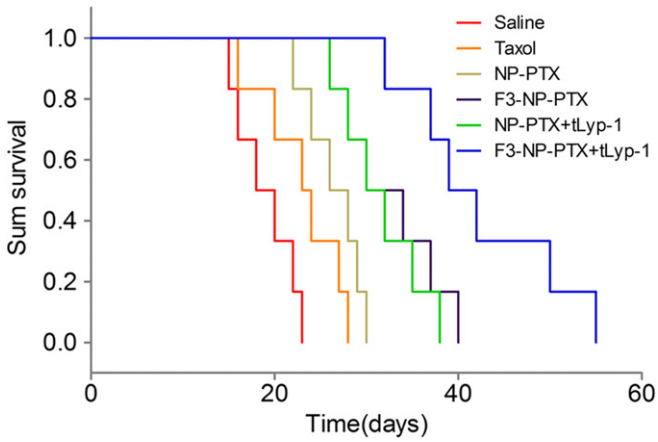

Fig. 9. Kaplan–Meier survival curve of mice bearing intracranial C6 glioma treated with Taxol®, NP-PTX, NP-PTX with co-administration of tLyp-1 peptide, F3-NP-PTX, F3-NP-PTX with co-administration of tLyP-1 peptide (PTX dose 5 mg/kg, tLyp-1 dose 4 μM/kg) and saline, respectively, every three days for two weeks. ($n = 6$).

For drug delivery system, nanoparticle size would be a precondition and a crucial factor which decide the fate of DDS both *in vivo* and *in vitro* [41]. In this contribution, NP size was perfectly controlled under 150 nm. The size between 100 nm and 200 nm was acknowledged as the best particle size for enhanced permeability and retention (EPR) effect which was the main mechanism for passive targeting of unmodified NP to tumor site [42,43]. After decorating NPs with F3 peptide via a maleimide–thiol coupling reaction, the particle size was found slightly increase but still under 150 nm with a narrow particle distribution. This F3 conjugation was also confirmed by the elevation of zeta potential from −32.5 ± 3.56 mV (NP) to −13.3 ± 1.32 mV (F3-NP). We believed this change was due to the electropositivity of F3 peptide.

In vitro PTX release experiment showed similar biphases release pattern for the NPs formulations [26,44]. In the first 6 h, a burst release was obtained. Ten hours later, a mild, sustained and under-controlled release was presented. The initial faster release was believed to be derived from the agents that located at the outer layer of the particles while the later slower one from that incorporated in the nanoparticle core and released in a prolonged way along with the erosion or degradation of the matrix.

In order to study the performance of F3 peptide-modified nanoparticulate DDS *in vitro*, series of cell experiments were conducted on C6 cells, a malignant mice glioma cell lines. Both qualitative and quantitative analysis showed that a significant higher cellular accumulation of F3-NP was detected when compared with unmodified NP, indicating that F3 peptide could effectively facilitate the interaction between the functionalized nanoparticles and C6 cells.

In the interaction between NPs and C6 cells, internalization mechanism would be a key step to be figured out in order to improve anti-tumor efficiency [45]. In this study, we incubated C6 cells with several different inhibitors to reveal the endocytosis mechanism of NP and F3-NP. As shown in Fig. 4, both the internalization of NPs and F3-NPs were significantly inhibited by M-β-CD which was regularly used to determine whether endocytosis was dependent on the integrity of lipid rafts [46], suggesting that the participation of lipid raft-mediated mechanism in the endocytosis of both NPs and F3-NPs. In the meanwhile, the internalization of F3-NPs was affected by nocodazole and BFA which were microtubules depolymerization agent and Golgi apparatus destroyer, respectively, indicating that in the involvement of cell skeleton and Golgi apparatus in the endocytosis of F3-NP. Taken the temperature-dependent experiment together, we claimed that the internalization of F3-NP was a Golgi apparatus involved, lipid raft-medicated and energy-dependent process. In addition, the internalization of F3-NPs but not NP could be inhibited by pre-incubation with free F3 peptide, suggesting that the improved C6 cellular association was mainly contributed by F3 conjugation.

In vitro cytotoxicity experiment was performed to evaluate the antiproliferative efficacy of F3-NP. The results showed that the IC_{50} of F3-NPs was 2.76 folds lower than that of NPs and 5.37 folds lower than that of Taxol®, suggesting that the antiproliferative effect of the drug-loaded nanoparticles was markedly elevated following the modification with F3 peptide. No significant difference was found between the cytoxicitity of F3-NP and F3-NP with tLyp-1. The antiproliferative results correlated well with the cellular uptake data, demonstrating that F3-conjunction could significantly improve C6 cellular association and anti-glioma efficacy.

Table 2
Pharmacokinetic parameters of PTX following intravenous administration of Taxol®, NP-PTX, F3-NP-PTX and F3-NP-PTX with tLyp-1 in SD rats at 5 mg/kg PTX dose and at 4 μM/kg tLyp-1 dose ($n = 3$).

Parameters	Taxol®	NP-PTX	F3-NP-PTX	F3-NP-PTX + tLyp-1
$AUC_{(0-t)}$ (μg/L/h)	3403	40345***	34530***	37370***
$K(h^{-1})$	0.30	0.11***	0.11***	0.10***
$T_{1/2}$ (h)	2.28	6.37**	6.41**	6.74**
CL (L/h)	1.48	0.12***	0.15***	0.13***

**$p < 0.01$, ***$p < 0.001$, significantly different with that of the Taxol® group.

Table 3
Median survival of mice bearing intracranial C6 glioma treated with Taxol®, NP-PTX, NP-PTX with co-administration of tLyp-1 peptide, F3-NP-PTX, F3-NP-PTX with co-administration of tLyP-1 peptide (PTX dose 5 mg/kg, tLyp-1 dose 4 μM/kg) and saline, respectively, every three days for two weeks.

Group	Median (day)	Standard error	Log-rank test (VS)				
			Saline	Taxol®	NP	F3-NP	tLyp-1 + NP
Saline	19	3.22	–	–	–	–	–
Taxol®	24	4.47	*	–	–	–	–
NP-PTX	27	3.08	**	*	–	–	–
F3-NP-PTX	32	5.43	***	**	*	–	–
tLyp-1 + NP-PTX	31	4.46	***	**	*	$p > 0.05$	–
tLyp-1 + F3-NP-PTX	42	8.55	***	***	***	*	**

*$p < 0.05$, **$p < 0.01$, ***$p < 0.001$, significantly different.

Multicell tumor spheroids were increasingly used to imitate the internal solid tumor tissue as it possessed several advantages that monolayer tumor cells could not provide. 3D tumor spheroids possess viable rim, with gradients of oxygen tension, nutrients, catabolites, and cell proliferation exactly the same as internal tumor microenvironment [47]. Here we used 3D multicell tumor spheroids as a glioma model to study the penetration ability of unmodified NPs and F3-NPs. The results showed that F3-NPs penetrated 139.26 μm, 1.72 times deeper than NP (81.02 μm), indicating F3-decoration DDS could be recognized and taken into the inner of solid tumor which was acknowledged as a key-step to cure the cancer. In contrast, co-administration with tumor-penetrating peptide tLyp-1 did not exhibit a strong role in promoting F3 conjugation DDS to penetrate into the tumor parenchyma. This was contradicted with the result of *in vivo* glioma distribution experiment, in which F3-NP with co-administration of tLyp-1 was found to achieve the most maximal accumulation and deepest penetration in the glioma region (Fig. 7D). In the meanwhile, co-administration with tLyp-1 peptide also facilitated the intra-glioma penetration of NP (Fig. 7A, B). Taken the *in vitro* and *in vivo* results together, we believed that the paradox could be contributed by differential expression of the receptor of tLyp-1–neuropilin-1 (NRP1) *in vitro* and *in vivo* (NRP1 was transmembrane protein mainly overexpressed on the surface of endothelial cells of neovasculature *in vivo*, but not on the avascular tumor spheroids *in vitro*). The lack of expression of NRP1 on glioma cells also contributed to the same antiproliferative effects of F3-NP-PTX and F3-NP-PTX with co-administration of tLyp-1.

Pharmacokinetic results showed that the PTX NPs formulations exhibited prolonged circulation time (half-life of 6.37 h and 6.41 h for NP-PTX and F3-NP-PTX, respectively), much slower plasma elimination rate (0.12 L/h and 0.15 L/h for NP-PTX and F3-NP-PTX, respectively) when compared with Taxol® (Fig. 8). In addition, after co-administration with tLyp-1 peptide, pharmacokinetic parameters of F3-NP did not show any change. Therefore, we claimed that F3 conjugation and co-administration with tLyp-1 peptide did not impair the stealth effects of the pegylated nanoparticulate DDS.

In vivo biodistribution was performed to evaluate the delivery efficiency of the different drug delivery strategies. Time-dependent biodistribution was studied by using a non-invasive NIR fluorescence imaging system. As shown in Fig. 6A, NP showed the maximum fluorescent intensity at 12 h, afterwards decreased at 24 h post-injection, suggesting that NP accumulation at tumor site mainly relied on EPR effect, which has been pointed out to take 7–8 h to achieve maximum accumulation at tumor site [48]. NP with co-administration of tLyp-1 peptide presented higher fluorescent intensity at the tumor site, indicating that taking tLyp-1 as the co-administration peptide was effective in facilitating DDS to locate and accumulate at the tumor location. Moreover, NP with tLyp-1 peptide showed higher fluorescent intensity at 6 h than 12 h, which further indicated tLyp-1 peptide as an effective supplementary to DDS based on its effect in mediating extravasation within minutes [49]. The biodistribution of F3-NP at the tumor region was slightly higher than that of NP with tLyp-1 and much higher than that of NP, confirming that the decoration with F3 peptide could significantly promote the tumor targeting and accumulation of DDS. F3-NP with co-administration of tLyp-1 exhibited a much superior accumulation at the glioma site than the other three formulations at all the time points, confirming that F3 peptide-modified nanoparticulate DDS could overcome blood–brain tumor barrier and enormously enhance anti-glioma efficiency especially when co-administrated with tLyp-1.

To evaluate anti-glioma efficiency, male Balb/c nude mice were xenografted with C6 glioma cells intracranially. One week after transplantation, the therapeutic schedule was set according to a pre-decided plan (every three days for two weeks at PTX dose of 5 mg/kg). A remarkable prolonged survival was observed in the mice treated with F3-NP with co-administration of tLyp-1 peptide, the medium survival time was 42 days, significantly higher than that of other treatments in both biological value and statistical point of view. NP co-administrated with tLyp-1 and F3-NP also enormously prolonged animal survival when compared with NP ($p < 0.05$), Taxol® ($p < 0.01$) and saline ($p < 0.001$). No significant difference was found between the NP with tLyp-1 and F3-NP groups. This result could be explained by their varied tumor accumulation pattern: NP with tLyp-1 showed a deeper glioma penetration while F3-NP exhibited a higher glioma accumulation (Fig. 7). The F3-decoration and tLyp-1 peptide co-administration resulted in enormous enhancement in the accumulation of PTX at the glioma region and thus significantly improved its anti-glioma efficacy.

5. Conclusion

For improving the anti-glioma drug delivery, a nanoparticulate drug delivery strategy was developed in this work by decorating pegylated polyester nanoparticles with F3 peptide and co-administrating the functionalized nanoparticles with a tumor homing and penetrating peptide, tLyp-1 peptide, to mediate efficient tumor targeting together with high cellular internalization and extensive vascular extravasation. The F3-NP displayed a uniformly spherical shape with particle size of 125 ± 11.12 nm and F3 peptide-conjugation confirmed by zeta potential determination and XPS analysis. Enhanced cellular interaction with C6 cells, improved penetration in 3D multicell tumor spheroids, and increased cytotoxicity of the loaded PTX were achieved by F3-NP. Following co-administration with tLyp-1 peptide, F3-NP exhibited enhanced accumulation at the tumor location and deep penetration into the glioma parenchyma. The longest survival in mice bearing intracranial C6 glioma was also achieved by co-administrating F3-NP with tLyp-1 peptide. These results suggested the drug delivery strategy by co-administrating a tumor homing and penetrating peptide with the glioma cells and neovasculature dual-targeting functionalized nanoparticles could significantly improve the anti-glioma drug delivery. The strategy might also provide a safer and more efficient platform for the treatment of other hard-to-treat tumors.

Acknowledgments

This work was supported by National Natural Science Foundation of China (81072592), National Key Basic Research Program (2013CB932502), National Science and Technology major Project (2012ZX09304004), Innovation Program of Shanghai Municipal Education Commission (12ZZ107), Program for New Century Excellent Talents in University and Grants from Shanghai Science and Technology Committee (11430702200, 12ZR1416300) and SJTU Funding (AE4160003). The authors also acknowledge the support from School of Pharmacy, Fudan University & the Open Project Program of Key Lab of Smart Drug Delivery (Fudan University), Ministry of Education & PLA, China (2011SDD-10).

References

[1] Wen PY, Kesari S. Malignant gliomas in adults. N Engl J Med 2008;359(5):492–507.
[2] Behin A, Hoang-Xuan K, Carpentier AF, Delattre JY. Primary brain tumours in adults. Lancet 2003;361(9354):323–31.
[3] Gladson CL, Prayson RA, Liu WM. The pathobiology of glioma tumors. Annu Rev Pathol 2010;5:33–50.
[4] Roger M, Clavreul A, Venier-Julienne MC, Passirani C, Montero-Menei C, Menei P. The potential of combinations of drug-loaded nanoparticle systems and adult stem cells for glioma therapy. Biomaterials 2011;32(8):2106–16.

[5] Ren J, Shen S, Wang D, Xi Z, Guo L, Pang Z, et al. The targeted delivery of anticancer drugs to brain glioma by PEGylated oxidized multi-walled carbon nanotubes modified with angiopep-2. Biomaterials 2012;33(11):3324–33.
[6] Beduneau A, Saulnier P, Benoit JP. Active targeting of brain tumors using nanocarriers. Biomaterials 2007;28(33):4947–67.
[7] Jiang X, Sha X, Xin H, Chen L, Gao X, Wang X, et al. Self-aggregated pegylated poly (trimethylene carbonate) nanoparticles decorated with c(RGDyK) peptide for targeted paclitaxel delivery to integrin-rich tumors. Biomaterials 2011;32(35):9457–69.
[8] Peer D, Karp JM, Hong S, Farokhzad OC, Margalit R, Langer R. Nanocarriers as an emerging platform for cancer therapy. Nat Nanotechnol 2007;2(12):751–60.
[9] McNeeley KM, Karathanasis E, Annapragada AV, Bellamkonda RV. Masking and triggered unmasking of targeting ligands on nanocarriers to improve drug delivery to brain tumors. Biomaterials 2009;30(23–24):3986–95.
[10] Shoichet MS, Winn SR. Cell delivery to the central nervous system. Adv Drug Deliv Rev 2000;42(1–2):81–102.
[11] Liu Y, Lu W. Recent advances in brain tumor-targeted nano-drug delivery systems. Expert Opin Drug Deliv 2012;9(6):671–86.
[12] Lammers T, Kiessling F, Hennink WE, Storm G. Drug targeting to tumors: principles, pitfalls and (pre-) clinical progress. J Control Release 2012;161(2): 175–87.
[13] Aktas Y, Yemisci M, Andrieux K, Gursoy RN, Alonso MJ, Fernandez-Megia E, et al. Development and brain delivery of chitosan-PEG nanoparticles functionalized with the monoclonal antibody OX26. Bioconjug Chem 2005;16(6): 1503–11.
[14] Xin H, Sha X, Jiang X, Zhang W, Chen L, Fang X. Anti-glioblastoma efficacy and safety of paclitaxel-loading Angiopep-conjugated dual targeting PEG-PCL nanoparticles. Biomaterials 2012;33(32):8167–76.
[15] Christian S, Pilch J, Akerman ME, Porkka K, Laakkonen P, Ruoslahti E. Nucleolin expressed at the cell surface is a marker of endothelial cells in angiogenic blood vessels. J Cell Biol 2003;163(4):871–8.
[16] Porkka K, Laakkonen P, Hoffman JA, Bernasconi M, Ruoslahti E. A fragment of the HMGN2 protein homes to the nuclei of tumor cells and tumor endothelial cells in vivo. Proc Natl Acad Sci U S A 2002;99(11):7444–9.
[17] Minchinton AI, Tannock IF. Drug penetration in solid tumours. Nat Rev Cancer 2006;6(8):583–92.
[18] Bhagat M, Halligan S, Sofou S. Nanocarriers to solid tumors: considerations on tumor penetration and exposure of tumor cells to therapeutic agents. Curr Pharm Biotechnol 2012;13(7):1306–16.
[19] Ruoslahti E. Peptides as targeting elements and tissue penetration devices for nanoparticles. Adv Mater 2012;24(28):3747–56.
[20] Sugahara KN, Teesalu T, Karmali PP, Kotamraju VR, Agemy L, Girard OM, et al. Tissue-penetrating delivery of compounds and nanoparticles into tumors. Cancer Cell 2009;16(6):510–20.
[21] Roth L, Agemy L, Kotamraju VR, Braun G, Teesalu T, Sugahara KN, et al. Transtumoral targeting enabled by a novel neuropilin-binding peptide. Oncogene 2012;31(33):3754–63.
[22] Xia H, Gao X, Gu G, Liu Z, Hu Q, Tu Y, et al. Penetratin-functionalized PEG-PLA nanoparticles for brain drug delivery. Int J Pharm 2012;436(1-2):840–50.
[23] Olivier JC, Huertas R, Lee HJ, Calon F, Pardridge WM. Synthesis of pegylated immunonanoparticles. Pharm Res 2002;19(8):1137–43.
[24] Yu DH, Lu Q, Xie J, Fang C, Chen HZ. Peptide-conjugated biodegradable nanoparticles as a carrier to target paclitaxel to tumor neovasculature. Biomaterials 2010;31(8):2278–92.
[25] Han LM, Guo J, Zhang LJ, Wang QS, Fang XL. Pharmacokinetics and biodistribution of polymeric micelles of paclitaxel with Pluronic P123. Acta Pharmacol Sin 2006;27(6):747–53.
[26] Xin H, Jiang X, Gu J, Sha X, Chen L, Law K, et al. Angiopep-conjugated poly(ethylene glycol)-co-poly(epsilon-caprolactone) nanoparticles as dual-targeting drug delivery system for brain glioma. Biomaterials 2011; 32(18):4293–305.
[27] Gao X, Yao L, Song Q, Zhu L, Xia Z, Xia H, et al. The association of autophagy with polyethylenimine-induced cytotoxicity in nephritic and hepatic cell lines. Biomaterials 2011;32(33):8613–25.
[28] Hirschhaeuser F, Menne H, Dittfeld C, West J, Mueller-Klieser W, Kunz-Schughart LA. Multicellular tumor spheroids: an underestimated tool is catching up again. J Biotechnol 2010;148(1):3–15.
[29] Xia H, Gao X, Gu G, Liu Z, Zeng N, Hu Q, et al. Low molecular weight protamine-functionalized nanoparticles for drug delivery to the brain after intranasal administration. Biomaterials 2011;32(36):9888–98.
[30] Guo J, Gao X, Su L, Xia H, Gu G, Pang Z, et al. Aptamer-functionalized PEG-PLGA nanoparticles for enhanced anti-glioma drug delivery. Biomaterials 2011;32(31):8010–20.
[31] Zeng N, Hu Q, Liu Z, Gao X, Hu R, Song Q, et al. Preparation and characterization of paclitaxel-loaded DSPE-PEG-liquid crystalline nanoparticles (LCNPs) for improved bioavailability. Int J Pharm 2012;424(1–2):58–66.
[32] Maher EA, Furnari FB, Bachoo RM, Rowitch DH, Louis DN, Cavenee WK, et al. Malignant glioma: genetics and biology of a grave matter. Genes Dev 2001; 15(11):1311–33.
[33] Biddlestone-Thorpe L, Marchi N, Guo K, Ghosh C, Janigro D, Valerie K, et al. Nanomaterial-mediated CNS delivery of diagnostic and therapeutic agents. Adv Drug Deliv Rev 2012;64(7):605–13.
[34] Petri B, Bootz A, Khalansky A, Hekmatara T, Muller R, Uhl R, et al. Chemotherapy of brain tumour using doxorubicin bound to surfactant-coated poly(butyl cyanoacrylate) nanoparticles: revisiting the role of surfactants. J Control Release 2007;117(1):51–8.
[35] Pang Z, Feng L, Hua R, Chen J, Gao H, Pan S, et al. Lactoferrin-conjugated biodegradable polymersome holding doxorubicin and tetrandrine for chemotherapy of glioma rats. Mol Pharm 2010;7(6):1995–2005.
[36] Zhan C, Wei X, Qian J, Feng L, Zhu J, Lu W. Co-delivery of TRAIL gene enhances the anti-glioblastoma effect of paclitaxel in vitro and in vivo. J Control Release 2012;160(3):630–6.
[37] Huang R, Ke W, Han L, Li J, Liu S, Jiang C. Targeted delivery of chlorotoxin-modified DNA-loaded nanoparticles to glioma via intravenous administration. Biomaterials 2011;32(9):2399–406.
[38] He H, Li Y, Jia XR, Du J, Ying X, Lu WL, et al. PEGylated poly(amidoamine) dendrimer-based dual-targeting carrier for treating brain tumors. Biomaterials 2011;32(2):478–87.
[39] Liu S, Guo Y, Huang R, Li J, Huang S, Kuang Y, et al. Gene and doxorubicin co-delivery system for targeting therapy of glioma. Biomaterials 2012;33(19): 4907–16.
[40] Gerstner ER, Batchelor TT. Antiangiogenic therapy for glioblastoma. Cancer J 2012;18(1):45–50.
[41] Alexis F, Pridgen E, Molnar LK, Farokhzad OC. Factors affecting the clearance and biodistribution of polymeric nanoparticles. Mol Pharm 2008;5(4): 505–15.
[42] Farokhzad OC, Langer R. Impact of nanotechnology on drug delivery. ACS Nano 2009;3(1):16–20.
[43] Torchilin V. Tumor delivery of macromolecular drugs based on the EPR effect. Adv Drug Deliv Rev 2011;63(3):131–5.
[44] Jiang X, Xin H, Sha X, Gu J, Jiang Y, Law K, et al. PEGylated poly(trimethylene carbonate) nanoparticles loaded with paclitaxel for the treatment of advanced glioma: in vitro and in vivo evaluation. Int J Pharm 2011;420(2): 385–94.
[45] Song Q, Yao L, Huang M, Hu Q, Lu Q, Wu B, et al. Mechanisms of transcellular transport of wheat germ agglutinin-functionalized polymeric nanoparticles in Caco-2 cells. Biomaterials 2012;33(28):6769–82.
[46] Brown DA, London E. Functions of lipid rafts in biological membranes. Annu Rev Cell Dev Biol 1998;14:111–36.
[47] McMahon KM, Volpato M, Chi HY, Musiwaro P, Poterlowicz K, Peng Y, et al. Characterization of changes in the proteome in different regions of 3D multicell tumor spheroids. J Proteome Res 2012;11(5):2863–75.
[48] Maeda H, Wu J, Sawa T, Matsumura Y, Hori K. Tumor vascular permeability and the EPR effect in macromolecular therapeutics: a review. J Control Release 2000;65(1–2):271–84.
[49] Sugahara KN, Teesalu T, Karmali PP, Kotamraju VR, Agemy L, Greenwald DR, et al. Coadministration of a tumor-penetrating peptide enhances the efficacy of cancer drugs. Science 2010;328(5981):1031–5.